SOCIETY FOR EXPERIMENTAL BIOLOGY

Journal of Experimental Botany, Vol. 72, No. 18 pp. 6087–6090, 2021
https://doi.org/10.1093/jxb/erab292 Advance Access Publication 16 June 2021
This paper is available online free of all access charges (see https://academic.oup.com/jxb/pages/openaccess for further details)

eXtra Botany

Viewpoint

The next phase in the development of ^{13}C isotopically non-stationary metabolic flux analysis

Thomas Wieloch*

Department of Medical Biochemistry and Biophysics, Umeå University, 901 87 Umeå, Sweden
* Correspondence: thomas.wieloch@umu.se

Editor: Johann Rohwer, Stellenbosch University, South Africa

^{13}C isotopically non-stationary metabolic flux analysis (^{13}C-INST-MFA) is an emerging technique for estimations of metabolic fluxes and pool sizes. Within the plant sciences, two studies utilizing this technique to characterize carbon metabolism have been published so far. Here, I examine these studies carefully. Readers unfamiliar with ^{13}C-INST-MFA will obtain a critical understanding of the method and its findings. Readers working with ^{13}C-INST-MFA are recommended to enter a phase of model validation to devise clear-cut protocols enabling robust estimations of specific fluxes.

Realistic reaction networks

In ^{13}C-INST-MFA, a list of coded reactions specifies by which routes carbon can move from labelled or unlabelled sources through metabolic networks into sinks (Fig. 1). The reaction network of both studies allows direct export of 3-phosphoglycerate (3PGA) from chloroplasts to the cytosol. In the light, however, 3PGA export is believed to be restricted due to the chloroplast to cytosol pH gradient (Flügge *et al.*, 1983, and references therein). Additionally, cytosolic reactions catalysed by glyceraldehyde-3-phosphate dehydrogenase and phosphoglycerate kinase are missing [conversion of glyceraldehyde 3-phosphate to 1,3-bisphosphoglycerate to 3PGA; triose phosphate (TP) to 3PGA]. Thus, ^{13}C flux into glycolysis and the tricarboxylic acid cycle may follow unrealistic routes and has no cytosolic connection with sucrose biosynthesis. Furthermore, fractional refixation of respired CO_2 is not considered (Loreto *et al.*, 1999), and numerous reversible reactions were programmed as irreversible, or *vice versa*. This includes reactions of the Calvin–Benson cycle catalysed by phosphoglycerate kinase and glyceraldehyde-3-phosphate dehydrogenase (conversion of 3PGA to 1,3-bisphosphoglycerate to glyceraldehyde 3-phosphate; 3PGA to TP), fructose bisphosphatase (conversion of fructose 1,6-bisphosphate to fructose 6-phosphate; FBP to F6P), and fructose-bisphosphate aldolase [conversion of dihydroxyacetone phosphate and erythrose 4-phosphate (E4P) to sedoheptulose 1,7-bisphosphate; TP and E4P to SBP]. Lastly, mesophyll chloroplasts reportedly lack enolase (van der Straeten *et al.*, 1991; Prabhakar *et al.*, 2009; Fukayama *et al.*, 2015). Thus, stromal conversion of 3PGA to phospho*enol*pyruvate (PEP) is likely to be infeasible, and fatty acid biosynthesis probably relies on PEP import from the cytosol. Future studies are encouraged to implement more realistic reaction networks representing carbon metabolism with all its intrinsic restrictions and freedom. Incorporation of cytosolic glyceraldehyde-3-phosphate dehydrogenases and phosphoglycerate kinase may enhance the utility of the model since these reactions proposedly constitute a central hub in leaf energy metabolism (Wieloch, 2021).

Constrained fluxes

INCA allows users to constrain fluxes and pool sizes, for example based on independent physiological measurements

Abbreviations: INCA, isotopomer network compartmental analysis; INST-MFA, isotopically non-stationary metabolic flux analysis; OPPP, oxidative pentose phosphate pathway; PEP, phospho*enol*pyruvate; 3PGA, 3-phosphoglycerate; R_L, day respiration; TP, triose phosphate; v_O/v_C, Rubisco oxygenation to carboxylation ratio; v_{OPPP}, OPPP flux; $v_{Sucrose}$, flux into sucrose; v_{Starch}, flux into starch.

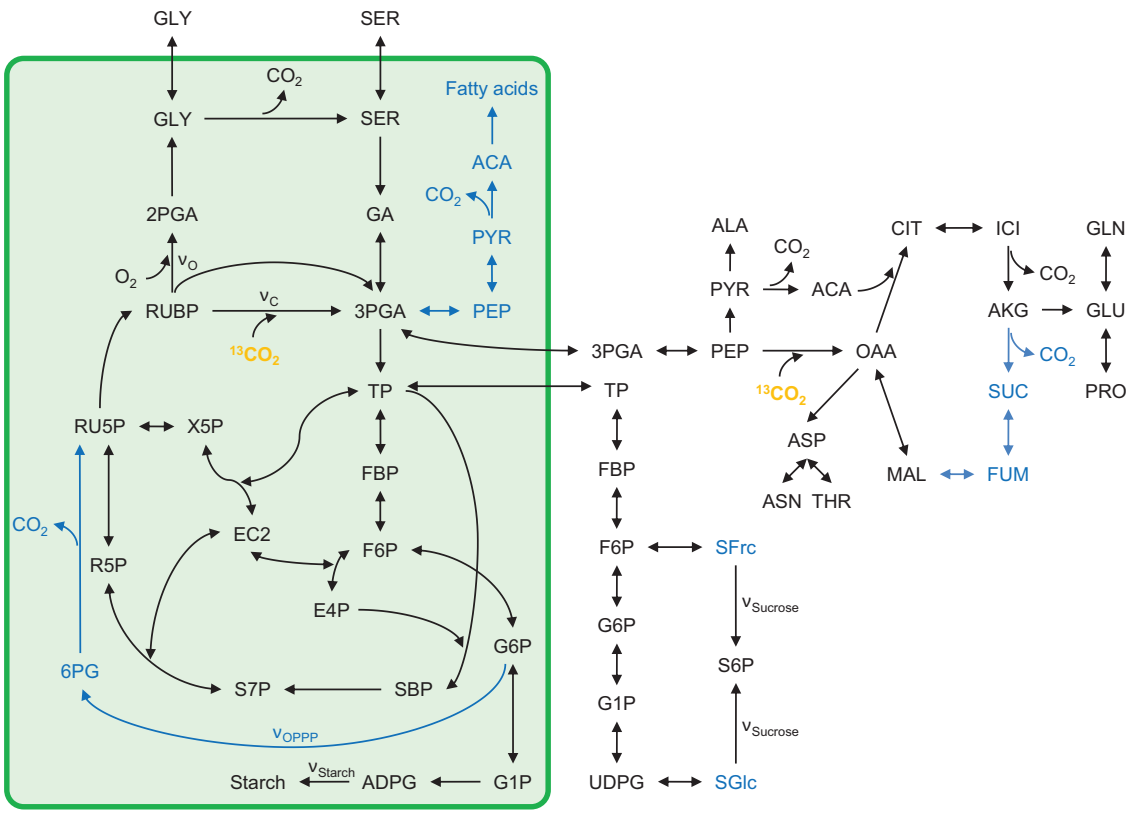

Fig. 1. Reaction networks of published ^{13}C-INST-MFA studies. Black: network as programmed by Ma *et al.* (2014; study 1) including reactions of the Calvin–Benson cycle, photorespiration, starch and sucrose biosynthesis, glycolysis, the tricarboxylic acid cycle, and amino acid biosynthesis. Blue: add-ons to the network of study 1 by Xu *et al.* (2021; study 2) including reactions of the oxidative pentose phosphate pathway, fatty acid biosynthesis, and the tricarboxylic acid cycle. Orange: ^{13}C-enriched compound (label) entering the reaction network. Reactions inside the green box were programmed as chloroplast localized, while reactions outside the box were programmed as either cytosolic or without a compartment identifier. Abbreviations: 2PGA, 2-phosphoglycerate; 3PGA, 3-phosphoglycerate; 6PG, 6-phosphogluconate; ACA, acetyl-CoA; ADPG, ADP-glucose; AKG, α-ketoglutarate; ALA, alanine; ASN, asparagine; ASP, aspartate; CIT, citrate; E4P, erythrose 4-phosphate; EC2, enzyme-bound two-carbon fragment; F6P, fructose 6-phosphate; FBP, fructose 1,6-bisphosphate; FUM, fumarate; G1P, glucose 1-phosphate; G6P, glucose 6-phosphate; GA, glycerate; GLN, glutamine; GLU, glutamate; GLY, glycine; ICI, isocitrate; MAL, malate; OAA, oxaloacetate; PEP, phospho*enol*pyruvate; PRO, proline; PYR, pyruvate; R5P, ribose 5-phosphate; RU5P, ribulose 5-phosphate; RUBP, ribulose 1,5-bisphosphate; S6P, sucrose 6-phosphate; S7P, sedoheptulose 7-phosphate; SBP, sedoheptulose 1,7-bisphosphate; SER, serine; SFrc, fructosyl moiety of S6P; SGlc, glucosyl moiety of S6P; SUC, succinate; THR, threonine; TP; triose phosphate (glyceraldehyde 3-phosphate and dihydroxyacetone phosphate); UDPG, UDP-glucose; X5P, xylulose 5-phosphate; ν_C, Rubisco carboxylation flux; ν_O, Rubisco oxygenation flux; ν_{OPPP}, OPPP flux; $\nu_{Sucrose}$, flux into sucrose; ν_{Starch}, flux into starch.

or theoretical considerations. Users may specify constants or intervals, or choose not to impose any constraints. In all models (both studies), net CO_2 assimilation was fixed at predetermined values scaling fluxes up to reasonable values (supporting interpretation of results) while maintaining flux ratios. Additionally, study 1 fixed the absolute flux into starch (Fig. 1, ν_{Starch}) and flux ratios between sucrose and amino acid biosynthesis according to physiological measurements. Similarly, study 2 fixed absolute fluxes into starch, sucrose ($\nu_{Sucrose}$), and amino acid biosynthesis, and the ratio of Rubisco oxygenation to carboxylation. This practice is potentially problematic since it may affect modelled flux ratios. Additionally, the necessity for constraints poses an important question. If large fluxes need to be fixed (ν_{Starch}, $\nu_{Sucrose}$, and ν_O/ν_C), can one rely on ^{13}C-INST-MFA to return credible results for unconstrained fluxes including smaller fluxes of interest (ν_{OPPP})? Thus, future studies are encouraged to present models without constraints alongside constrained models to show that data-driven flux estimation is feasible. Ideally, ^{13}C data should drive the estimations with a minimum of imposed constraints.

Effects of constrained fluxes on fluxes of interest

In principle, constraining fluxes or pool sizes can affect estimates of fluxes or pool sizes of interest due to interconnectivities within the reaction network (Fig. 1). In study 2, ν_O/ν_C was constrained to be between 0.2 and 0.25. Modelling returned a ν_O/ν_C ratio of 0.2, and an R_L and ν_{OPPP} of 5.2 μmol CO_2 g^{-1} FW h^{-1} and 4.6 μmol CO_2 g^{-1} FW h^{-1}, respectively. When left unconstrained, modelling returned a physiologically unrealistic ν_O/ν_C ratio of 0.09, and an

R_L and v_{OPPP} of 12.1 μmol CO_2 g^{-1} FW h^{-1} and 10.5 μmol CO_2 g^{-1} FW h^{-1}, respectively. This indicates negative correlations between v_O/v_C and R_L and v_O/v_C and v_{OPPP} (the lower photorespiration, the higher day respiration). Hence, fixing v_O/v_C at values >0.2 may cause $R_L \rightarrow 0$ and $v_{OPPP} \rightarrow 0$. Note that under normal growth conditions, v_O/v_C ratios of 0.34 are common (Sharkey, 1988; Cegelski and Schaefer, 2006; Pärnik *et al.*, 2007). Thus, future studies are encouraged to include sensitivity analyses investigating dependence between constrained fluxes and fluxes of interest.

Validation of results by independent methods

INCA-based ^{13}C-INST-MFA returns a comprehensive dataset containing estimates of (i) forward and reverse fluxes of all reactions and (ii) pool sizes of all metabolites specified in the reaction network (Fig. 1). Some of these items are accessible to other analytical techniques which, in principle, enables independent validation of ^{13}C-INST-MFA results. Study 1 made no attempt to confirm modelled v_O/v_C estimates by independent methods. However, estimated ratios were within the physiologically reasonable range. In contrast, study 2 tested the model estimate for R_L (5.2 μmol CO_2 g^{-1} FW h^{-1}) by the Laisk method which returned an R_L estimate of 9.3 μmol CO_2 g^{-1} FW h^{-1} (Brooks and Farquhar, 1985). However, corresponding 95% confidence intervals showed no overlap (3.5–8.05 μmol CO_2 g^{-1} FW h^{-1} versus 8.1–10.7 μmol CO_2 g^{-1} FW h^{-1}). Thus, these estimates are statistically different at the 0.05 significance level. Additionally, the model estimate for v_{OPPP} in chloroplasts was compared with an estimate of flux through the cytosolic OPPP (Sharkey *et al.*, 2020). However, there is no reason to believe that these pathways carry the same flux. Thus, validation of estimates from ^{13}C-INST-MFA by independent methods has not yet been achieved. However, independently determined fluxes currently used as constraints (v_{Starch} and $v_{Sucrose}$) can be utilized to test the method by leaving them unconstrained and comparing modelled and measured values. Additionally, v_O/v_C ratios may help to test the method since several alternative methods can provide independent estimates (Busch, 2013).

Metabolically inactive pools or injection of carbon from unlabelled sources

In ^{13}C-INST-MFA, ^{12}C is progressively flushed out of the metabolic network and replaced by ^{13}C from the labelling compound, such as $^{13}CO_2$ (Fig. 1). Both studies reported fast initial labelling of metabolite pools. After several minutes, however, labelling slowed and, even after 1 h, a significant fraction of the pools remained unlabelled. This was attributed to metabolically inactive pools (i.e. metabolite pools disconnected from the flux of incoming ^{13}C) and modelled accordingly by including a dilution term for each metabolite (accounting for apparently constant offsets between measured and modelled ^{13}C enrichments). Alternatively, labelling lags may be explained in combination by breakdown of weakly labelled cytosolic sucrose into glucose and fructose, phosphorylation by hexokinase and fructokinase, and reinjection of glucose-6-phosphate-derived carbon into chloroplasts via a cytosolic OPPP not shown in Fig. 1 (Sharkey *et al.*, 2020). Figure 2 shows reported ^{13}C enrichments of metabolites of the Calvin–Benson cycle, and starch and sucrose biosynthesis 1 h into $^{13}CO_2$ labelling of *Arabidopsis thaliana* rosettes (Szecowka *et al.*, 2013). Additionally, these authors reported subcellular distributions of metabolites given on the *x*-axis from fully plastidial (x=0) to fully cytosolic (x=1). Interestingly, plastidial metabolites are more strongly ^{13}C labelled than cytosolic metabolites. Metabolite distribution explains 55% of the labelling variability (P<0.01, n=11). Since it is not apparent why sizes of metabolically inactive pools would correlate with plastid–cytosol metabolite distribution, this corroborates the idea of injection of weakly labelled carbon into cytosolic metabolism. Future ^{13}C-INST-MFA studies are encouraged to further explore this by expanding their reaction networks by sucrose breakdown pathways and a cytosolic OPPP. Additionally, sucrose, glucose, and fructose are large carbon pools with significant vacuolar contributions (Szecowka *et al.*, 2013). Thus, cytosol–vacuole transmembrane transport of these metabolites may need to be considered.

Future focus

To date, evidence that ^{13}C-INST-MFA returns reliable flux and pool size estimates is not available. Therefore, the field is recommended to enter a phase of validation of the complex models used in ^{13}C-INST-MFA to devise clear-cut protocols enabling robust estimations of specific fluxes.

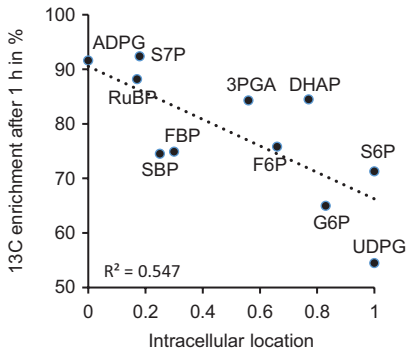

Fig. 2. ^{13}C enrichment of metabolite pools in *Arabidopsis thaliana* rosettes 1 h into $^{13}CO_2$ labelling as a function of the intracellular metabolite distribution from fully plastidial (x=0) to fully cytosolic (x=1). Abbreviations: 3PGA, 3-phosphoglycerate; ADPG, ADP-glucose; DHAP, dihydroxyacetone phosphate; F6P, fructose 6-phosphate; FBP, fructose 1,6-bisphosphate; G6P, glucose 6-phosphate; RuBP, ribulose 1,5-bisphosphate; S6P, sucrose 6-phosphate; S7P, sedoheptulose 7-phosphate; SBP, sedoheptulose 1,7-bisphosphate; UDPG, UDP-glucose. Re-analysed data from Szecowka *et al.* (2013). Sucrose and glucose 1-phosphate were excluded from the analysis since the former has a large vacuolar fraction and the latter reportedly exhibits an anomalous labelling behaviour (Szecowka *et al.*, 2013; Xu *et al.*, 2021).

Data availability

The data supporting the findings of this study have been published by Ma *et al.* (2014), Szecowka *et al.* (2013), and Xu *et al.* (2021).

Keywords: Carbon flux estimation, carbon metabolism, ^{13}C labelling, $^{13}CO_2$, complex models, ^{13}C tracer experiments, labelling lag, metabolic flux analysis, model validation, photosynthesis.

References

Brooks A, Farquhar GD. 1985. Effect of temperature on the CO_2/O_2 specificity of ribulose-1,5-bisphosphate carboxylase/oxygenase and the rate of respiration in the light. Planta **165**, 397–406.

Busch FA. 2013. Current methods for estimating the rate of photorespiration in leaves. Plant Biology **15**, 648–655.

Cegelski L, Schaefer J. 2006. NMR determination of photorespiration in intact leaves using *in vivo* $^{13}CO_2$ labeling. Journal of Magnetic Resonance **178**, 1–10.

Cheah YE, Young JD. 2018. Isotopically nonstationary metabolic flux analysis (INST-MFA): putting theory into practice. Current Opinion in Biotechnology **54**, 80–87.

Flügge UI, Gerber J, Heldt HW. 1983. Regulation of the reconstituted chloroplast phosphate translocator by an H^+ gradient. Biochimica et Biophysica Acta **725**, 229–237.

Fukayama H, Masumoto C, Taniguchi Y, Baba-Kasai A, Katoh Y, Ohkawa H, Miyao M. 2015. Characterization and expression analyses of two plastidic enolase genes in rice. Bioscience, Biotechnology, and Biochemistry **79**, 402–409.

Loreto F, Delfine S, Di Marco G. 1999. Estimation of photorespiratory carbon dioxide recycling during photosynthesis. Functional Plant Biology **26**, 733–736.

Ma F, Jazmin LJ, Young JD, Allen DK. 2014. Isotopically nonstationary ^{13}C flux analysis of changes in *Arabidopsis thaliana* leaf metabolism due to high light acclimation. Proceedings of the National Academy of Sciences, USA **111**, 16967–16972.

Ma F, Jazmin LJ, Young JD, Allen DK. 2017. Isotopically nonstationary metabolic flux analysis (INST-MFA) of photosynthesis and photorespiration in plants. In: Fernie AR, Bauwe H, Weber APM, eds. Photorespiration: methods and protocols. New York: Springer, 167–194.

Pärnik T, Ivanova H, Keerberg O. 2007. Photorespiratory and respiratory decarboxylations in leaves of C_3 plants under different CO_2 concentrations and irradiances. Plant, Cell & Environment **30**, 1535–1544.

Prabhakar V, Löttgert T, Gigolashvili T, Bell K, Flügge UI, Häusler RE. 2009. Molecular and functional characterization of the plastid-localized phosphoenolpyruvate enolase (ENO1) from *Arabidopsis thaliana*. FEBS Letters **583**, 983–991.

Sharkey TD. 1988. Estimating the rate of photorespiration in leaves. Physiologia Plantarum **73**, 147–152.

Sharkey TD, Preiser AL, Weraduwage SM, Gog L. 2020. Source of ^{12}C in Calvin–Benson cycle intermediates and isoprene emitted from plant leaves fed with $^{13}CO_2$. The Biochemical Journal **477**, 3237–3252.

Szecowka M, Heise R, Tohge T, *et al.* 2013. Metabolic fluxes in an illuminated *Arabidopsis* rosette. The Plant Cell **25**, 694–714.

Van der Straeten D, Rodrigues-Pousada RA, Goodman HM, Van Montagu M. 1991. Plant enolase: gene structure, expression, and evolution. The Plant Cell **3**, 719–735.

Wieloch T. 2021. A cytosolic oxidation–reduction cycle in plant leaves. Journal of Experimental Botany **72**, 4186–4189.

Xu Y, Fu X, Sharkey TD, Shachar-Hill Y, Walker BJ. 2021. The metabolic origins of non-photorespiratory CO_2 release during photosynthesis: a metabolic flux analysis. Plant Physiology **186**, 297–314.

Young JD. 2014. INCA: a computational platform for isotopically nonstationary metabolic flux analysis. Bioinformatics **30**, 1333–1335.